

Size-dependent ferroic phase transformations in GeSe nanoribbons

Cite as: Appl. Phys. Lett. **121**, 122903 (2022); <https://doi.org/10.1063/5.0111375>

Submitted: 19 July 2022 • Accepted: 07 September 2022 • Published Online: 21 September 2022

 Yang Yang,  Hongxiang Zong,  Xiangdong Ding, et al.



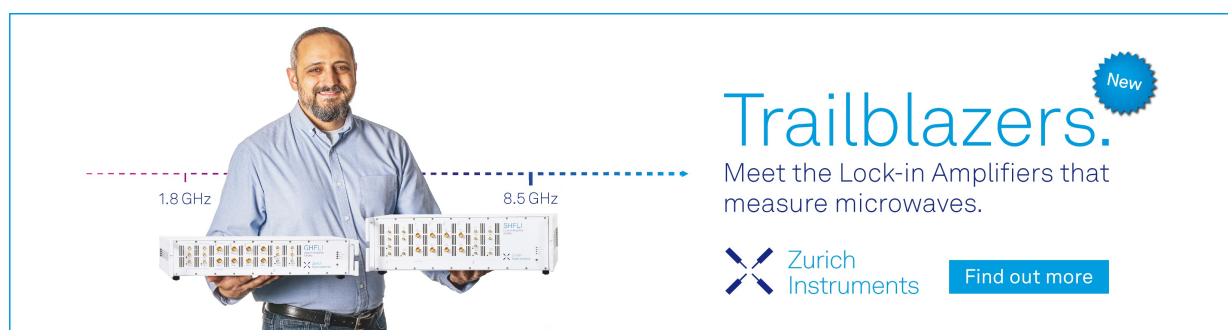
View Online




Export Citation




CrossMark

Trailblazers. 

Meet the Lock-in Amplifiers that measure microwaves.

 Zurich Instruments [Find out more](#)

Size-dependent ferroic phase transformations in GeSe nanoribbons

Cite as: Appl. Phys. Lett. **121**, 122903 (2022); doi: [10.1063/5.0111375](https://doi.org/10.1063/5.0111375)

Submitted: 19 July 2022 · Accepted: 7 September 2022 ·

Published Online: 21 September 2022



View Online



Export Citation



CrossMark

Yang Yang,  Hongxiang Zong,  Xiangdong Ding,  and Jun Sun

AFFILIATIONS

State Key Laboratory for Mechanical Behavior of Materials, Xi'an Jiaotong University, Xi'an 710049, China

^{a)} Authors to whom correspondence should be addressed: zonghust@mail.xjtu.edu.cn and dingxd@mail.xjtu.edu.cn

ABSTRACT

Ferroic phase transformation in monolayer nanosheets or nanoribbons endows 2D nanoelectronic devices with novel functionalities. However, less is known how the phase transformation behaves with the system size. Combined with molecular dynamic simulations and a machine learning model, we systematically investigate the temperature induced ferroic phase transformation in monolayer GeSe nanoribbons, which exhibits remarkable size effect. Specifically, the transformation hysteresis is found continuously decreased with ribbon width at the investigated scales. In contrast, the transformation temperature of monolayer GeSe nanoribbons shows non-monotonic size-dependency, i.e., it is first increased and then decreased as we narrow the GeSe nanoribbons. We attribute this to a competition between the enhanced ripple deformation, which will promote phase transformation upon cooling, and the stronger edge effect that can suppress phase transformation. In addition, the two factors are well captured by the Landau model, which will deepen our understanding of phase transformation behaviors in 2D ferroic materials.

Published under an exclusive license by AIP Publishing. <https://doi.org/10.1063/5.0111375>

The past two decades have witnessed the fantastic discoveries of multifunctional two-dimensional (2D) materials.^{1–5} Among them, 2D ferroic materials, such as 1T' WTe₂,⁶ black phosphorene,⁷ and group IV monochalcogenides,^{8–10} exhibit fascinating properties due to the ferroic phase transformation and domain switching. Group IV monochalcogenides,^{8–11} e.g., GeSe monolayers, as a typical 2D multiferroic material, show strongly coupled ferroelastic–ferroelectric orders. Below the phase transformation temperature [typically <300 K (Ref. 11)], it shows spontaneous strain or polarization and domain patterns,⁹ which have been observed experimentally,^{12–14} serving as an ideal case to understand the phase transformation behaviors in 2D materials.

A class of native structures named ripples,¹⁵ which originated from the low-energy flexural out-of-plane bending mode, widely exist in 2D materials, including 2D ferroic materials.^{10,15–19} Different from the static ripples induced by the deformed substrate in 3D bulk membranes, ripples in 2D materials are intrinsic and with ultrafast dynamics.¹⁹ Static ripples in 3D bulk ferroic membranes induced an out-of-plane strain field, resulting in a strong room-temperature ferroelectricity²⁰ and enhanced piezoelectricity.²¹ However, the understanding of the dynamic rippling effects in 2D ferroics is still far from complete. Our previous work focused on the dynamic rippling effects on the phase transformation and domain switching in monolayer

GeSe. We have indicated that the ripple deformation can help stabilize a low-temperature ferroic phase and increase the phase transformation temperatures.¹⁰ Nevertheless, it is still unknown what the rippling effects look like in 2D ferroics with limited sizes (i.e., with free edges).

Free edges or surfaces work for the size effects of ferroic materials. For example, the structural phase transformation in 3D shape memory materials (typical ferroelastic materials) shows strong dependence of system size at the small scale. Previous studies also demonstrate that shape memory alloys (SMAs) can exhibit different properties at the small scale than their bulk counterparts, as manifested by suppressed phase transformation temperatures,²² and slim thermal or superelastic hysteresis in nanoscale SMAs.^{23,24} The decreasing phase transformation hysteresis comes from the weak spontaneous strain and spatial heterogeneity in smaller systems, which results in a quasi-continuous phase transformation process.²⁴ However, less is known whether it is the same true for 2D shape memory or ferroic materials.

2D ferroic materials possess several unique aspects that are different from that in 3D bulk materials.²⁵ Often, 2D ferroic materials have a thickness of several atomic layers, which gives rise to strong surface effects along the out-of-plane direction. Cutting the 2D nanosheet of ferroic materials into nanoribbons leads to additional changes from edge effect. Furthermore, 2D materials are featured by a unique

flexible bending mode, resulting in inborn ripple deformation.^{10,15–19} The motivation of this work is to understand how these effects change with the system size and their role in the phase transformations of 2D ferroic materials.

In the present work, molecular dynamics (MD) simulation is carried out to study structural phase transformations in monolayer GeSe nanoribbons, aimed at achieving an atomic-level understanding of the size effect on 2D shape memory materials. The atomic interaction in monolayer GeSe is described by a machine learning potential that is directly learned from high-accuracy first-principle calculations.¹⁰ Our previous work has shown that the machine learning potential can exactly reproduce the ferroic phase transformation and domain switching processes in GeSe monolayer. Typical GeSe nanoribbons are created with a system size of 15.9 nm in length and 4.0–17.0 nm in width, containing up to 6400 atoms. The periodic boundary condition is only applied along the nanoribbons while the other two directions are bounded by two free surfaces. All the samples are first relaxed at 200 K by using a Nose–Hoover thermostat^{26,27} and a Parrinello–Rahman barostat²⁸ within the isothermal–isobaric ensemble. After this procedure, we performed MD simulations of cooling and heating on the annealed samples utilizing the LAMMPS code.²⁹ The cooling and heating processes involve a cyclic increase or decrease in temperature with rates of 0.5 K/ps. The complete details of the machine learning model and the code for LAMMPS implementation have been uploaded to <https://github.com/yangymse/GeSe-MLPotential.git>.

Figure 1(a) shows the crystal structure of the low-temperature ferroic phase, whose formation can be characterized by the changes in the lattice parameters a and b as well as the relative in-plane displacement vector between Ge–Se pairs (Δx , Δy). The local lattice-invariant shear (i.e., a – b) differs ferroelastic domains or variants with different symmetry-equivalent directions of structural distortion while the

displacement vector of (Δx , Δy) quantifies local spontaneous polarization, as shown in Fig. 1(b). The GeSe monolayer has four different variants associated with the symmetry change upon phase transformation at low temperatures. In Fig. 1(c), we show a single ferroelastic domain with local spontaneous strain along the y direction after the phase transformation, and the arrows represent local spontaneous polarization. Note that the spatial distribution of local spontaneous strain and spontaneous polarization is correlated, indicating a strong coupling between them.^{7,9} Therefore, either one in our case can be used as the order parameter of phase transformation in monolayer GeSe. At high temperatures, both order parameters in monolayer GeSe lost their long-range order [Fig. 1(d)], which suggest the occurrence of a structural phase transformation upon heating. Even so, we still can see very weak short-range ferroic order in a high-temperature phase due to the presence of local ripple deformation.¹⁰

Our work started by studying the stable monolayer GeSe nanoribbons. Here, both the armchair and zigzag edged GeSe nanoribbons are considered. As shown in Fig. S1, we designed two types of pristine monolayer GeSe nanoribbons with either armchair or zigzag edges. When undergoing phase transformation upon heating or cooling, the edges in both cases transform into zigzag. It indicates that the zigzag edge is more stable in monolayer GeSe nanoribbons. This is further confirmed by the edge energy calculation. By means of first principles calculations, we show that the zigzag edged nanoribbon has an edge formation energy of 903 meV/nm, which is lower than that of armchair edged nanoribbons (1182 meV/nm). Therefore, our study hereafter will focus on the zigzag edged GeSe nanoribbons.

Figure 2 shows the size dependence of phase transformation behaviors in GeSe nanoribbons. In detail, zigzag edged GeSe nanoribbons with ribbon width varying from 4 to 16 nm as well as a freestanding GeSe nanosheet are involved in our MD simulations. Figure 2(a) shows the temperature dependent mean lattice parameters a and b upon heating and cooling. The difference between a and b reflects the symmetry change associated with the phase transformation in GeSe. Under cooling, both a and b decrease smoothly with temperature. Then a discontinuous change occurs due to the occurrence of a first-order phase transformation. The corresponding phase transformation temperature is defined as the martensitic starting temperature (M_s). Similarly, when we heat the samples, the a and b vary continuously first and then coincide at the reverse phase transformation temperature, which is known as the austenite finishing temperature (A_f). Usually, the austenite finishing temperature is higher than the martensitic starting temperature, and their difference can be used to evaluate the phase transformation hysteresis ($A_f - M_s$).

Figure 2(b) shows the forward and reverse transformation temperatures (M_s and A_f , respectively) of the GeSe nanoribbons. Compared with the monolayer GeSe nanosheet [~ 320 K, as shown in Fig. 2(a)], A_f in GeSe nanoribbons is slightly decreased first. However, the change in A_f becomes sharp as the nanoribbons are narrower than 8 nm. More differently, the size dependence of M_s shows a “ Λ ” shape. With reducing width of GeSe nanoribbons, the M_s first rises above 8 nm and then decreases sharply. It is important to note that such non-monotonic size dependency of M_s has never been observed in bulk shape memory materials.²⁴ Moreover, the transformation hysteresis ΔT (here, we define $\Delta T = A_f - M_s$) becomes smaller with reducing size, as shown in Fig. 2(c), be consistent with previous observations in shape memory alloys.²⁴

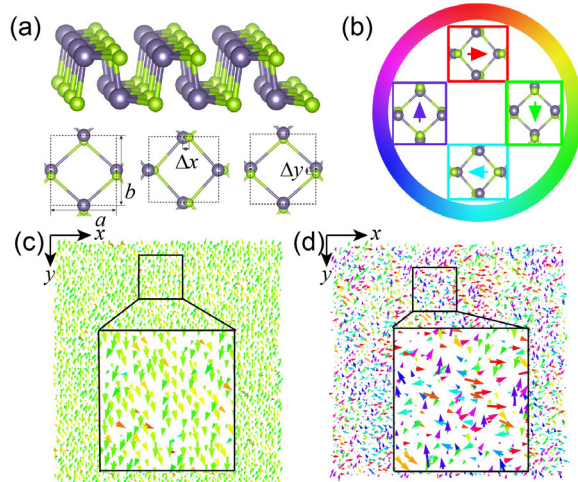


FIG. 1. Structural changes upon the phase transformation in monolayer GeSe. (a) Atomistic configurations and selected order parameter in ferroic monolayer GeSe. (b) The four symmetry-equivalent directions of structural distortion in the low-temperature phase are indicated by the displacement vector of (Δx , Δy). (c) Single domain structure of the low temperature phase. (d) High temperature phase with weak short-range ferroic order. The arrows represent relative in-plane displacement of (Δx , Δy) between Ge–Se pairs.

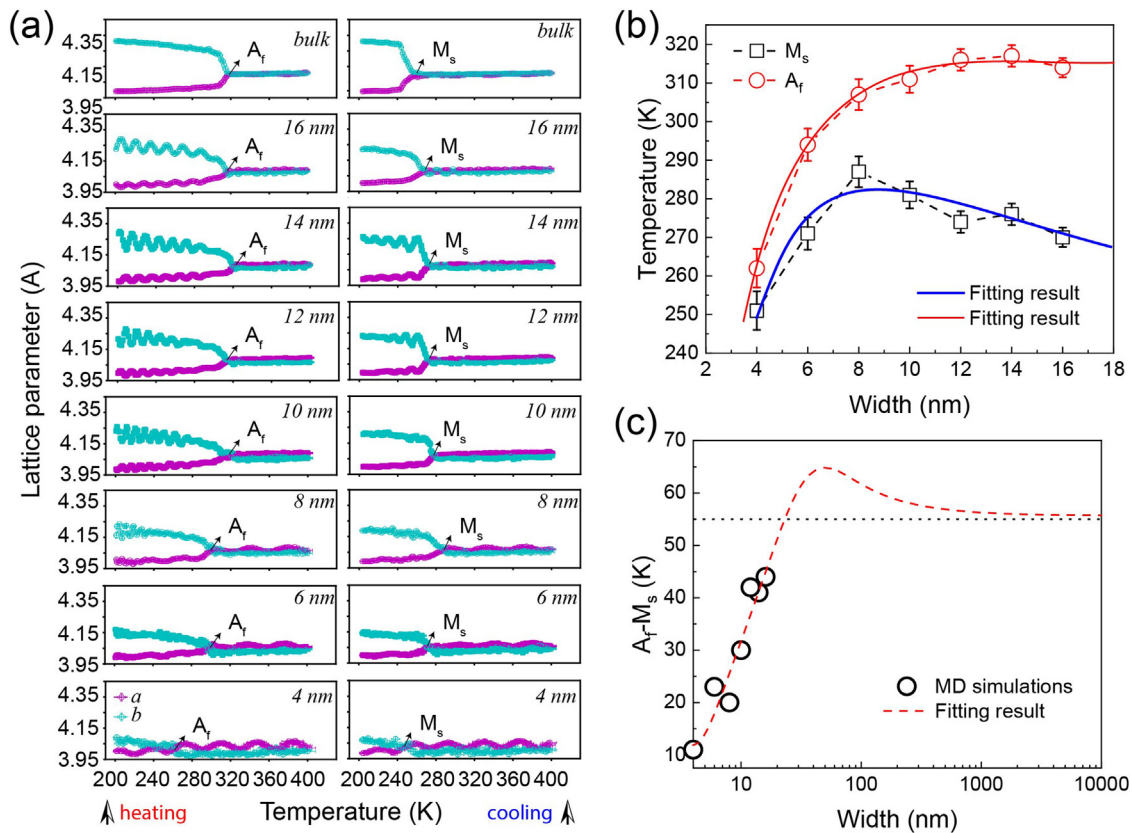


FIG. 2. Size dependency of ferroic phase transformations in monolayer GeSe nanoribbons. (a) Mean lattice parameters as a function of temperature upon heating and cooling. (b) The nanoribbon width-dependent transformation temperatures (M_s and A_f). The Landau-type analysis model showing the relationship between M_s (blue solid line) and A_f (red solid line) and ribbon width. They agree well with the MD simulation results. (c) The corresponding transformation hysteresis as a function of the ribbon width during the forward and reverse phase transformations. Once the system is approaching the bulk limit, the hysteresis saturated at 55 K (red dashed line).

To reveal the microscopic nature of size effect, we investigate the corresponding microstructure evolution upon heating and cooling in a GeSe nanoribbon. By examining multiple snapshots stored during the MD simulations, we find that the phase transformation process in GeSe nanoribbons is strongly related to the regions near the ribbon edges. As shown in the upper panel of Fig. 3, the high-temperature phase prefers to nucleate from the near-edge regions upon heating and then grow into the whole sample [Figs. 3(a)–3(d)]. In contrast, when we decrease the temperature from a high-temperature phase region, the low-temperature phase prefers to nucleate from the ribbon inner, instead of the edges. A further cooling leads to the entirely low-temperature phase with a multidomain structure, see the lower panel of Figs. 3(e)–3(h). Even so, the spontaneous strain or polarization in the near-edge regions is much weaker than the center place. Our findings, thus, suggest that the edge plays an important role in the phase transformation process in 2D GeSe nanoribbons.

Coincidentally, previous results found that surface regions dominate the phase transformation in nanoscale shape memory materials.²² Accordingly, we calculated the formation energy of ribbon edges in martensite (γ^M) and austenite (γ^A). In our MD simulations, the edge formation energy is calculated by $\gamma_{\text{edge}} = (E_{\text{free}} - E_{\text{peri}})/N$, where E_{free} represents the total potential energy of a GeSe nanoribbon system

while E_{peri} is the corresponding potential energy of GeSe bulk, and N is the atom number of the system. As expected, the edge formation energy in the low-temperature phase (γ^M) is higher than that in the high-temperature phase (γ^A). This indicates that the spontaneous strain/polarization on the edges should be suppressed. Additional energetic price should be paid for the formation of the low-temperature phase in the near-edge regions. In other words, the low-temperature phase prefers to nucleate at the inner ribbon upon cooling while the high-temperature phase will start from the edges during the heating process. However, the nucleation of the high-temperature phase in the near-edge region will be energetically preferred compared to its bulk counterpart. Furthermore, we find that the edge formation energy difference ($\Delta\gamma$) between low-temperature and high-temperature phases is enlarged with decreasing sample size, as shown in Fig. 4(a). It should justify the suppressed phase transformation in narrower GeSe nanoribbons.

The out-of-plane deformation or ripple deformation in 2D materials makes additional contribution to the change of phase transformations in GeSe nanoribbons. Ripples are intrinsic crystal defects in 2D materials and involve locally with time and space.¹⁹ This dynamic local deformation can induce local strain that facilitates local phase transformation in monolayer GeSe.¹⁰ To uncover the role of ripple

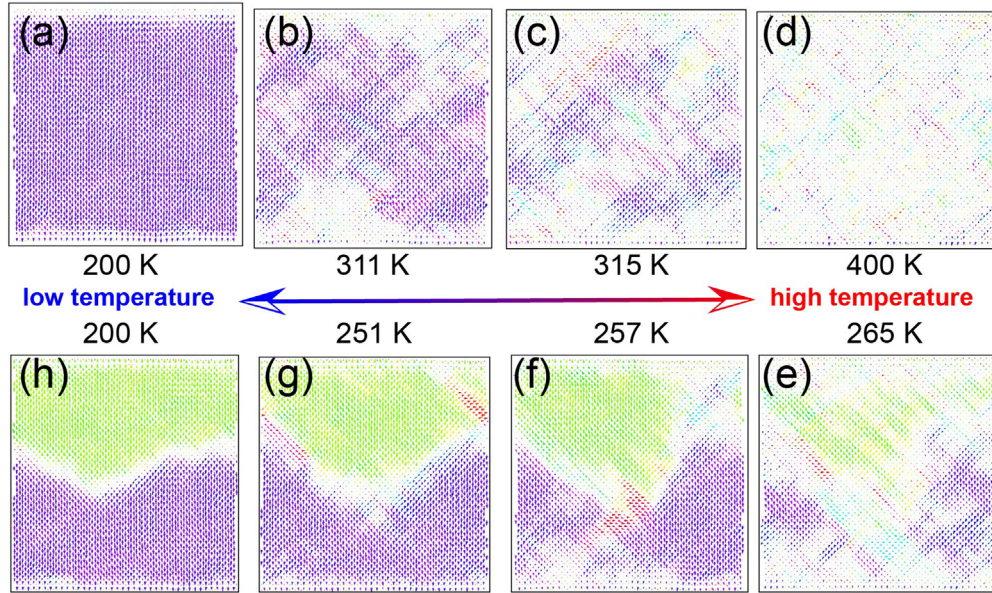


FIG. 3. Typical atomic configurations of a GeSe nanoribbon with zigzag edges upon heating and cooling. (a) Original single domain structure. (b)–(d) Nucleation and growth of the high-temperature phase upon heating. (e)–(h) Nucleation and growth of the low-temperature phase upon cooling.

deformation in GeSe nanoribbons, we evaluate the intensity of ripple deformation as a function of the system size. Here, both the Gaussian curvature κ and out-of-plane fluctuations³⁰ $\langle h^2 \rangle / S_0$ (S_0 refers to the initial area of the sample) due to ripple deformation are estimated, as shown in Figs. S2 and S3. Both increase exponentially with the reduction in the ribbon width, indicating that the out-of-plane ripple deformation roughly follows an exponential relationship with the system size [Figs. 4(b) and S3(c)]. As presented in our previous work,¹⁰ ripples introduce a local random strain field, which can give rise to dynamic low-temperature phase nanoregions even at high temperatures. The presence of ripples can extend the lifetime of the local low-temperature phase about 100 times longer. With such enhanced ripple deformation at smaller sample, the low-temperature phase can be more stable at a higher temperature. It explains the increased M_s in narrower GeSe nanoribbons below 8 nm in Fig. 2(b). Aside from the size-dependency, previous studies have shown that ripple deformation follows a linear relationship with temperature.^{10,30}

Thus, by taking account of the two factors, we propose a Landau-type model to study generally the structural phase transformations in monolayer GeSe nanoribbons. Previous studies have indicated that the surface/edge effect can be described by a phenomenological parameter, i.e., extrapolation length δ (>0) to characterize the near-edge region, which favors the high-temperature phase.^{23,24} The contribution of ripple deformation is related to additional strain energy due to phase transformation. Based on these, the Landau free energy of structural phase transformation in 2D materials can be expressed as

$$F = \frac{1}{2}A\eta^2 + \frac{1}{4}B\eta^4 + \frac{1}{6}C\eta^6 + \frac{1}{2}s(\nabla\eta)^2 + r(W, T)\eta, \quad (1)$$

where η is the order parameter; A , B , and C are parameters related to the materials; A can be expressed as $A_0(T - T_c)$; $\frac{1}{2}s(\nabla\eta)^2$ is related to the surface inhibition to the martensitic phase transformation. $r(W, T)$

is the strain field induced by ripple deformation, where W and T refer to the ribbon width and temperature, respectively. Our previous work has shown that the strength of a local strain field $r(W, T)$ is a linear function of order parameter η and temperature T .¹⁰ By using a similar strategy shown in Ref. 22 (see the [supplementary material](#)), the relationship between the martensitic phase transformation start temperature M_s and the ribbon width W can be obtained as

$$M_s = T_c^M - \frac{2s}{\delta W A_0} + \frac{1}{A_0} e^{mW}. \quad (2)$$

The austenite phase transformation finish temperature can be obtained as

$$A_f = T_c^A - \frac{2s}{\delta W A_0'} + \frac{1}{A_0'} e^{m'W}. \quad (3)$$

As shown in Fig. 2(b), we fit the simulation results with Eqs. (2) and (3), and the low fitting error indicates that our model can well capture the size dependence of phase transformation in GeSe nanoribbons.

The hysteresis ($A_f - M_s$) can be easily derived by substituting Eqs. (R1) and (R2), leading to the following equation:

$$A_f - M_s = (T_c^A - T_c^M) + p \cdot W^{-1} + q \cdot e^{lW}, \quad (4)$$

where p , q , and l are the reduced coefficients.

As Eq. (4) suggested, once the system is approaching the bulk limit, the hysteresis saturated at 55 K [Fig. 2(c)] agrees well with our MD simulations.

Based on the analytical model, the structural phase transformations of real SMAs at nanoscale and their critical sizes could be estimated since the parameters in the present model can be obtained from experiments. The extrapolation length δ can be measured directly from high-resolution TEM images while other parameters can be

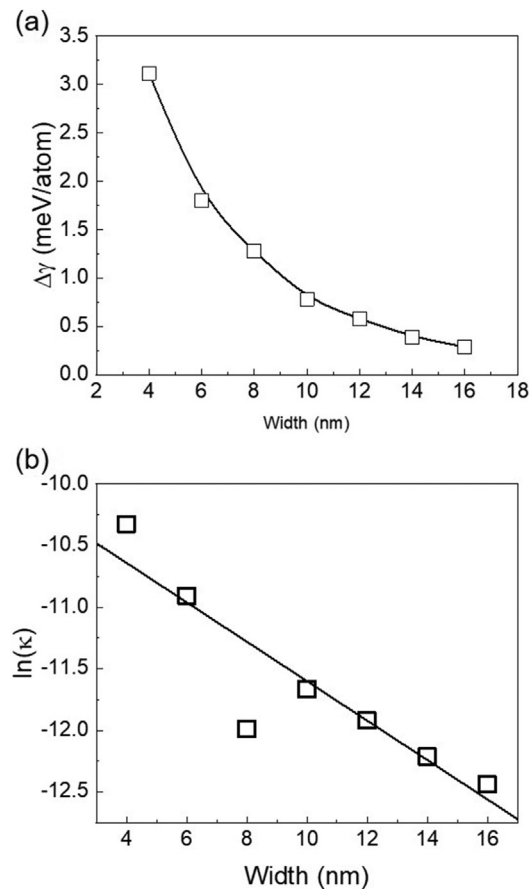


FIG. 4. Size effect on the (a) edge formation energy difference and (b) mean Gaussian curvature in GeSe nanoribbons.

obtained from the transformation properties of bulk materials. However, the Landau model cannot capture the effects of layer-thickness on the phase transformation. Thickness effects include: first, the adjacent layers should have opposite ferroelectric order parameters but the same ferroelastic order parameters. In this scenario, only samples with odd layers show ferroelectricity.^{12,14} Second, the ripple deformation is also thickness dependent.³¹ Unfortunately, the current machine learning model cannot easily capture the interaction between GeSe layers, which could be studied in the future.

In summary, we have investigated the temperature induced ferroic phase transformation in 2D GeSe nanoribbons, which shows strong size-dependency. Different from that in 3D shape memory materials, the phase transformation temperature shows non-monotonic size dependency in 2D GeSe nanoribbons. Atomic level investigations point out that the anomalous size effect results from a competition between the cost of additional edge formation energy and the promotion of ripple deformation induced local strain. The latter is unique for 2D shape memory materials. Due to the structural transformation in wide 2D ferroic materials, our findings potentially have board applications in 2D functional nanosystems such as shape memory effect and ferroelectric and magnetocaloric systems.

See the [supplementary material](#) for more details of the reconstruction of armchair free edge, size dependent curvature, and out-of-plane fluctuations as well as the derivation of the Landau-type model.

This work was supported by the National Natural Science Foundation of China (Nos. 12104355, 51320105014, 51871177, and 51931004), the China Postdoctoral Science Foundation (No. 2020M673385), and the 111 project 2.0 (No. BP2018008).

AUTHOR DECLARATIONS

Conflict of Interest

The authors have no conflicts to disclose.

Author Contributions

Yang Yang: Investigation (equal); Methodology (equal); Writing – original draft (equal). **Hongxiang Zong:** Investigation (equal); Methodology (equal); Writing – review & editing (equal). **XiangDong Ding:** Project administration (equal); Supervision (equal); Writing – review & editing (equal). **Jun Sun:** Project administration (equal); Supervision (equal).

DATA AVAILABILITY

The data that support the findings of this study are available from the corresponding authors upon reasonable request.

REFERENCES

- ¹K. S. Novoselov, A. K. Geim, S. V. Morozov, D. Jiang, Y. Zhang, S. V. Dubonos, I. V. Grigorieva, and A. A. Firsov, *Science* **306**(5696), 666 (2004).
- ²K. S. Novoselov, A. Mishchenko, A. Carvalho, and A. H. Castro Neto, *Science* **353**(6298), aac9439 (2016).
- ³W. Choi, N. Choudhary, G. H. Han, J. Park, D. Akinwande, and Y. H. Lee, *Mater. Today* **20**(3), 116 (2017).
- ⁴Y. Cao, V. Fatemi, A. Demir, S. Fang, S. L. Tomarken, J. Y. Luo, J. D. Sanchez-Yamagishi, K. Watanabe, T. Taniguchi, and E. Kaxiras, *Nature* **556**(7699), 80 (2018).
- ⁵Y. Cao, V. Fatemi, S. Fang, K. Watanabe, T. Taniguchi, E. Kaxiras, and P. Jarillo-Herrero, *Nature* **556**(7699), 43 (2018).
- ⁶W. Li and J. Li, *Nat. Commun.* **7**, 10843 (2016).
- ⁷M. Wu and X. C. Zeng, *Nano Lett.* **16**(5), 3236 (2016).
- ⁸R. Fei, W. Kang, and L. Yang, *Phys. Rev. Lett.* **117**(9), 097601 (2016).
- ⁹H. Wang and X. Qian, *2D Mater.* **4**(1), 015042 (2017).
- ¹⁰Y. Yang, H. Zong, J. Sun, and X. Ding, *Adv. Mater.* **33**(49), 2103469 (2021).
- ¹¹M. Mehboudi, B. M. Fregoso, Y. Yang, W. Zhu, A. van der Zande, J. Ferrer, L. Bellaiche, P. Kumar, and S. Barraza-Lopez, *Phys. Rev. Lett.* **117**(24), 246802 (2016).
- ¹²Y. Bao, P. Song, Y. Liu, Z. Chen, M. Zhu, I. Abdelwahab, J. Su, W. Fu, X. Chi, and W. Yu, *Nano Lett.* **19**(8), 5109 (2019).
- ¹³N. Higashitarumizu, H. Kawamoto, C.-J. Lee, B.-H. Lin, F.-H. Chu, I. Yonemori, T. Nishimura, K. Wakabayashi, W.-H. Chang, and K. Nagashio, *Nat. Commun.* **11**(1), 2428 (2020).
- ¹⁴K. Chang, J. Liu, H. Lin, N. Wang, K. Zhao, A. Zhang, F. Jin, Y. Zhong, X. Hu, and W. Duan, *Science* **353**(6296), 274 (2016).
- ¹⁵A. Fasolino, J. H. Los, and M. I. Katsnelson, *Nat. Mater.* **6**, 858 (2007).
- ¹⁶Y. Wang, R. Yang, Z. Shi, L. Zhang, D. Shi, E. Wang, and G. Zhang, *ACS Nano* **5**(5), 3645 (2011).
- ¹⁷L. Tapasztó, T. Dumitrica, S. J. Kim, P. Nemes-Incze, C. Hwang, and L. P. Biro, *Nat. Phys.* **8**(10), 739 (2012).
- ¹⁸A. Kushima, X. Qian, P. Zhao, S. Zhang, and J. Li, *Nano Lett.* **15**(2), 1302 (2015).
- ¹⁹J. Hu, G. M. Vanacore, A. Cepellotti, N. Marzari, and A. H. Zewail, *Proc. Natl. Acad. Sci. U. S. A.* **113**(43), E6555 (2016).

- ²⁰T. Li, S. Deng, H. Liu, S. Sun, H. Li, S. Hu, S. Liu, X. Xing, and J. Chen, *Adv. Mater.* **33**(21), 2008316 (2021).
- ²¹G. Dong, S. Li, T. Li, H. Wu, T. Nan, X. Wang, H. Liu, Y. Cheng, Y. Zhou, W. Qu, Y. Zhao, B. Peng, Z. Wang, Z. Hu, Z. Luo, W. Ren, S. J. Pennycook, J. Li, J. Sun, Z.-G. Ye, Z. Jiang, Z. Zhou, X. Ding, T. Min, and M. Liu, *Adv. Mater.* **32**(50), 2004477 (2020).
- ²²Z. Zhang, X. Ding, J. Deng, J. Cui, J. Sun, T. Suzuki, K. Otsuka, and X. Ren, *J. Phys. Chem. C* **117**(15), 7895 (2013).
- ²³Z. Zhang, X. Ding, J. Sun, T. Suzuki, T. Lookman, K. Otsuka, and X. Ren, *Phys. Rev. Lett.* **111**(14), 145701 (2013).
- ²⁴H. Zong, Z. Ni, X. Ding, T. Lookman, and J. Sun, *Acta Mater.* **103**, 407 (2016).
- ²⁵R. Mas-Balleste, C. Gomez-Navarro, J. Gomez-Herrero, and F. Zamora, *Nanoscale* **3**(1), 20 (2011).
- ²⁶S. Nosé, *J. Chem. Phys.* **81**(1), 511 (1984).
- ²⁷W. G. Hoover, *Phys. Rev. A* **31**(3), 1695 (1985).
- ²⁸M. Parrinello and A. Rahman, *J. Appl. Phys.* **52**(12), 7182 (1981).
- ²⁹S. Plimpton, *J. Comput. Phys.* **117**(1), 1 (1995).
- ³⁰W. Gao and R. Huang, *J. Mech. Phys. Solids* **66**, 42 (2014).
- ³¹S. Li, Q. Li, R. W. Carpick, P. Gumbsch, X. Z. Liu, X. Ding, J. Sun, and J. Li, *Nature* **539**(7630), 541 (2016).